

# Discussion of Cold Nuclear Matter Effects on Quarkonium Production

R. Vogt

Physics Division, Lawrence Livermore National Laboratory, Livermore, CA  
94551, USA

Physics Department, University of California, Davis, CA 95616, USA

# What Are Cold Matter Effects?

Important cold nuclear matter effects include:

- Initial-state nuclear effects on the parton densities (shadowing)
- Initial-state energy loss
- Intrinsic heavy flavors
- Final-state absorption on nucleons

Shadowing and absorption most important at midrapidity, initial-state energy loss and intrinsic heavy flavor more important at forward rapidity

Production mechanism affects both intimately:

- Shadowing depends on momentum fraction  $x$  of the target (and projectile in  $AA$ ) which is influenced by how the state was produced:  $2 \rightarrow 1$  or  $2 \rightarrow 2$  process
- Production affects absorption because singlet and octet states can be absorbed differently

# Quarkonium Production Issues

# Numerous Production Models

## Color Evaporation Model (CEM):

Hadronization scale  $k = \mathcal{O}(\Lambda_{\text{QCD}})$ ,  $Q\bar{Q}$  quantum numbers changed by soft interactions with probabilities specific to each state but independent of energy (Barger *et al.*; Gavai *et al.*; Schuler and RV)

## Color Singlet Model I (CSM):

$k = \mathcal{O}(m_Q)$ , singlet states with correct quantum numbers; hard gluon needed for  $S$  states, *e.g.*  $gg \rightarrow J/\psi g$ ;  $gg \rightarrow \chi_{c2}$  dominant? (Baier *et al.*; Schuler)

## Nonrelativistic QCD (NRQCD) – alias Color Octet Model:

$k = \mathcal{O}(\alpha_s m_Q)$ ,  $Q\bar{Q}$  quantum numbers changed via gluon emission at bound state momentum scale; corresponds to velocity  $v = k/m_Q$  expansion; nonperturbative octet and singlet matrix elements fit to data (Braaten, Bodwin and Lepage; Cho and Leibovich; Beneke and Rothstein; Maltoni *et al.* ...)

## Color Singlet Model II (CSM\*):

$k = \mathcal{O}(\sqrt{\hat{s}})$ , new contributions from heretofore neglected “ $s$ -channel cut” diagrams for  $S$  states (Lansberg *et al.*)

## Comover Enhancement Scenario (CES):

$k = \mathcal{O}(1/\tau_{\text{AP}})$ ,  $1/m_Q \leq \tau_{\text{AP}} \leq 1/\Lambda_{\text{QCD}}$ ,  $Q\bar{Q}$  quantum numbers changed by perturbative interactions with comoving color field (Hoyer and Peigne)

## Intrinsic Charm:

$k$  typically assumed to be soft,  $gc \rightarrow J/\psi c$  provides additional source of high  $p_T$ , forward  $J/\psi$  production (Brodsky and Lansberg)

# Color Evaporation Model

All quarkonium states are treated like  $Q\bar{Q}$  ( $Q = c, b$ ) below  $H\bar{H}$  ( $H = D, B$ ) threshold  
Distributions for all quarkonium family members identical. Production ratios  
should also be independent of  $\sqrt{s}$ ,  $p_T$ ,  $x_F$ .

At LO,  $gg \rightarrow Q\bar{Q}$  and  $q\bar{q} \rightarrow Q\bar{Q}$ ; NLO add  $gq \rightarrow Q\bar{Q}q$

$$\sigma_Q^{\text{CEM}} = F_Q \sum_{i,j} \int_{4m_Q^2}^{4m_H^2} d\hat{s} \int dx_1 dx_2 f_{i/p}(x_1, \mu^2) f_{j/p}(x_2, \mu^2) \hat{\sigma}_{ij}(\hat{s}) \delta(\hat{s} - x_1 x_2 s)$$

Values of  $m_Q$  and  $Q^2$  fixed from NLO calculation of  $Q\bar{Q}$  production

Inclusive  $F_Q$  fixed by comparison of NLO calculation of  $\sigma_Q^{\text{CEM}}$  to  $\sqrt{s}$  dependence of  
 $J/\psi$  and  $\Upsilon$  cross sections,  $\sigma(x_F > 0)$  and  $Bd\sigma/dy|_{y=0}$  for  $J/\psi$ ,  $Bd\sigma/dy|_{y=0}$  for  $\Upsilon$

Data and branching ratios used to separate the  $F_Q$ 's for each quarkonium state

Resonance	$J/\psi$	$\psi'$	$\chi_{c1}$	$\chi_{c2}$	$\Upsilon$	$\Upsilon'$	$\Upsilon''$	$\chi_b(1P)$	$\chi_b(2P)$
$\sigma_i^{\text{dir}}/\sigma_H$	0.62	0.14	0.6	0.99	0.52	0.33	0.20	1.08	0.84
$f_i$	0.62	0.08	0.16	0.14	0.52	0.10	0.02	0.26	0.10

Table 1: The ratios of the direct quarkonium production cross sections,  $\sigma_i^{\text{dir}}$ , to the inclusive  $J/\psi$  and  $\Upsilon$  cross sections, denoted  $\sigma_H$ , and the feed down contributions of all states to the  $J/\psi$  and  $\Upsilon$  cross sections,  $f_i$ , Digal *et al.*.

# CEM $J/\psi$ and $\Upsilon$ Total Cross Sections

Energy dependence obtained from NLO  $Q\bar{Q}$  cross section below open heavy flavor threshold, parton densities and phase space

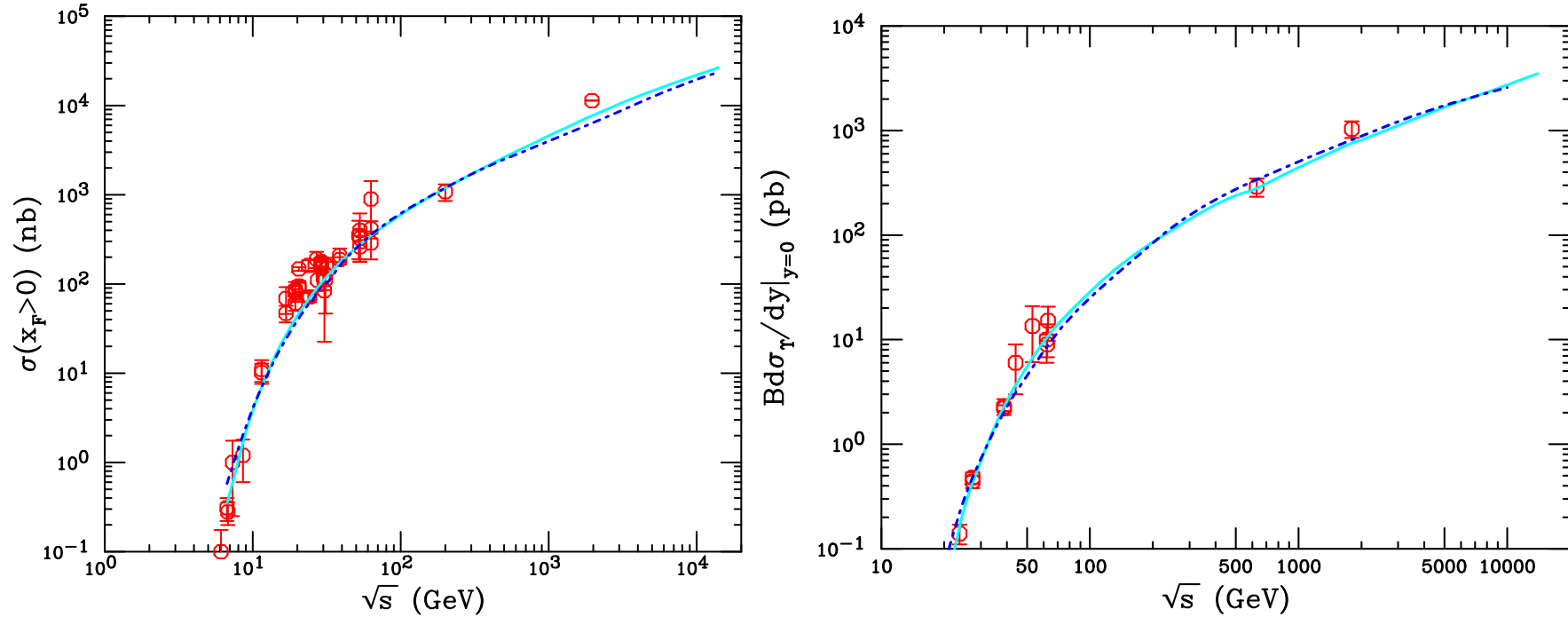


Figure 1: The  $J/\psi$  forward cross sections (left) and the combined  $\Upsilon S$  states in the dilepton channel (right) calculated to NLO in the CEM. The solid cyan curve employs the MRST HO distributions while the dot-dashed blue curve is a result with CTEQ6M. Both take  $m_c = 1.2$  GeV and  $m_\Gamma = 2\sqrt{p_{T,Q\bar{Q}}^2 + m_c^2}$  for  $J/\psi$  and  $m_b = 4.75$  GeV and  $m_\Gamma = \sqrt{p_{T,Q\bar{Q}}^2 + m_c^2}$ . [After Phys. Rept. 458 (2008) 1.]

## CEM $p_T$ Distributions in the $Q\bar{Q}$ NLO Code

Without intrinsic  $k_T$  smearing (or resummation) the  $Q\bar{Q}$   $p_T$  distribution (LO at  $\mathcal{O}(\alpha_s^3)$  while total cross section is NLO at this order) is too peaked at  $p_T \rightarrow 0$ , needs broadening at low  $p_T$

Implemented by Gaussian  $k_T$  smearing,  $\langle k_T^2 \rangle_p = 1 \text{ GeV}^2$  for fixed target  $pp$  and  $\pi p$ , broadened for  $pA$  and  $AA$ , NLO code adds in final state:

$$g_p(k_T) = \frac{1}{\pi \langle k_T^2 \rangle_p} \exp(-k_T^2 / \langle k_T^2 \rangle_p)$$

Comparison with  $J/\psi$  and  $\Upsilon$  Tevatron data at 1.8 TeV shows that the broadening should increase with energy; we make a simple linear extrapolation to obtain

$$\langle k_T^2 \rangle_p = 1 + \frac{1}{3} \ln \left( \frac{\sqrt{s}}{\sqrt{s_0}} \right) \text{ GeV}^2$$

Thus at RHIC energies, with  $\sqrt{s_0} = 20 \text{ GeV}$ , expect  $\langle k_T^2 \rangle_p = 1.77 \text{ GeV}^2$  for 200 GeV and 2.07  $\text{GeV}^2$  for 500 GeV  $pp$  collisions; can test this

## Comparison to CDF Run II Quarkonium Data

Default calculation with  $\langle k_T^2 \rangle = 2.53 \text{ GeV}^2$  from high  $p_T$  Run I data may be too strong,  $\langle k_T^2 \rangle = 1.76 \text{ GeV}^2$  works better

Data may support even lower  $\langle k_T^2 \rangle$  values, rather low average  $p_T$  for data

Normalization assumes inclusive  $J/\psi$ , no rapidity bin width included, scaled up to agree with total forward cross section on previous slide

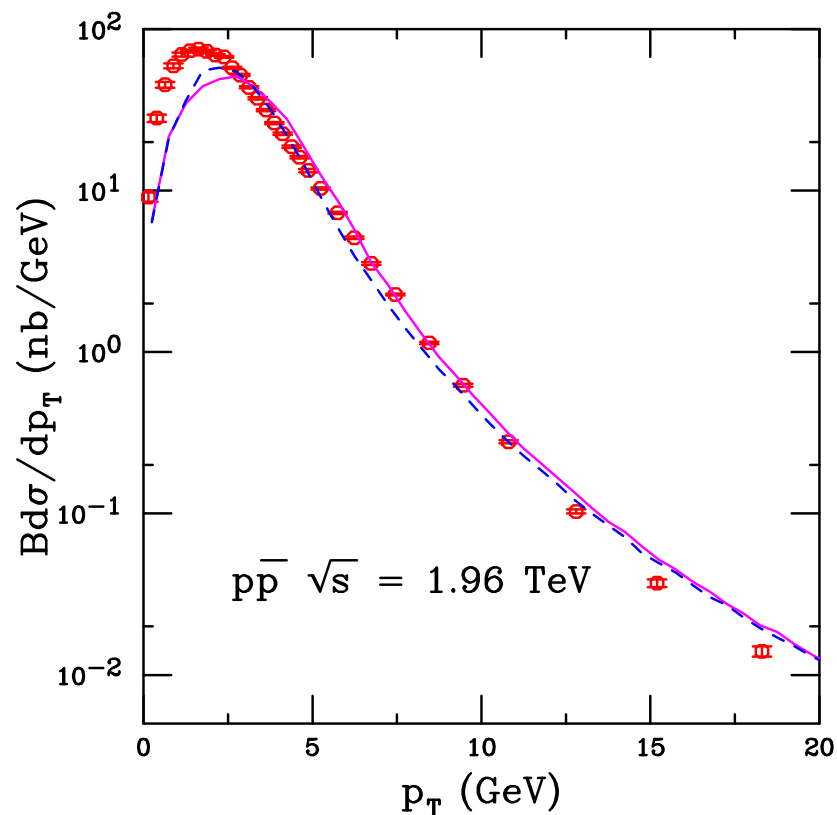


Figure 2: The  $J/\psi$   $p_T$  distributions compared to CDF data at  $\sqrt{s} = 1.96 \text{ TeV}$  for  $\langle k_T^2 \rangle = 2.53$  (solid magenta) and  $1.76$  (dashed blue)  $\text{GeV}^2$ . [After G. Schuler and R.V., Phys. Lett. B **387** (1996) 181.] There is an additional factor of 1.8 in the normalization to agree with the total cross section, assuming inclusive  $J/\psi$  and that the rapidity bin width is not included.

# CEM Comparison to RHIC $pp$ $J/\psi$ Data

CEM calculation reproduces shape of  $J/\psi$   $p_T$  and  $y$  distributions rather well  
Normalization is also rather good, 'fudge' factor of 1.3 to match data

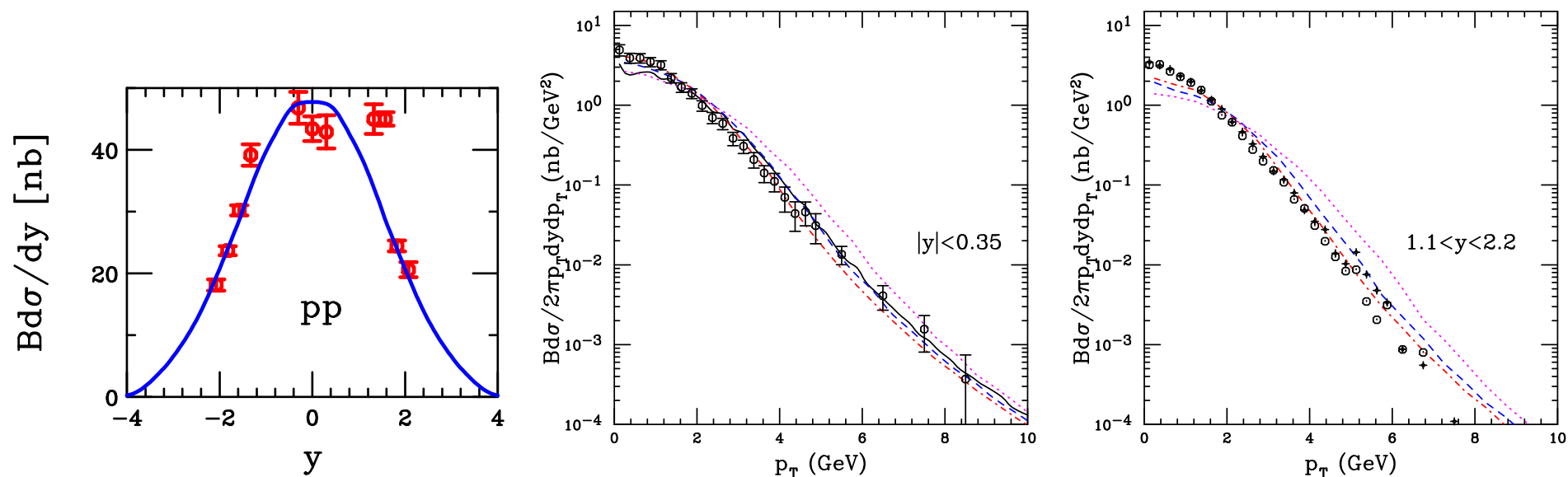


Figure 3: PHENIX  $pp$  measurements compared to CEM calculation at  $\sqrt{s} = 200$  GeV. The  $J/\psi$  rapidity distribution (left) and transverse momentum distributions at midrapidity (center) and in the muon arms (right). The solid black line in the center is a previous calculation with the MRST HO PDFs. The blue dashed, red dot-dashed and magenta dotted curves correspond to  $\langle k_T^2 \rangle = 1.77$  GeV<sup>2</sup> (default kick), 1.38 GeV<sup>2</sup> (half default kick) and 2.53 GeV<sup>2</sup> (twice default kick).

# Predictions for $\Upsilon$ Production at RHIC

Branching ratio to leptons not included; inclusive  $\Upsilon(1S)$  distributions

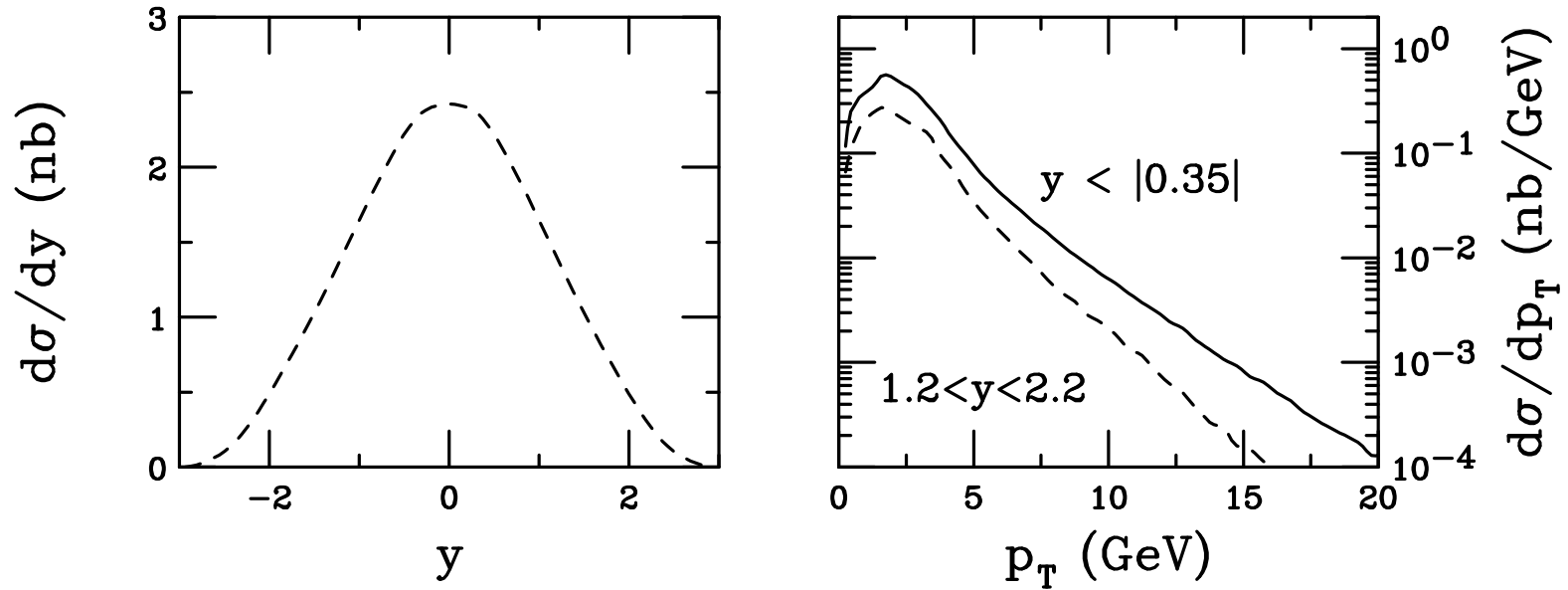


Figure 4: The inclusive  $\Upsilon$  rapidity (left) and  $p_T$  distributions (right) at  $\sqrt{s} = 200$  GeV. The  $p_T$  distributions at mid- and forward rapidity are shown.

# Quarkonium Predictions for 500 GeV $pp$ Production

Less difference between mid and forward rapidity  $p_T$  distributions at higher energy

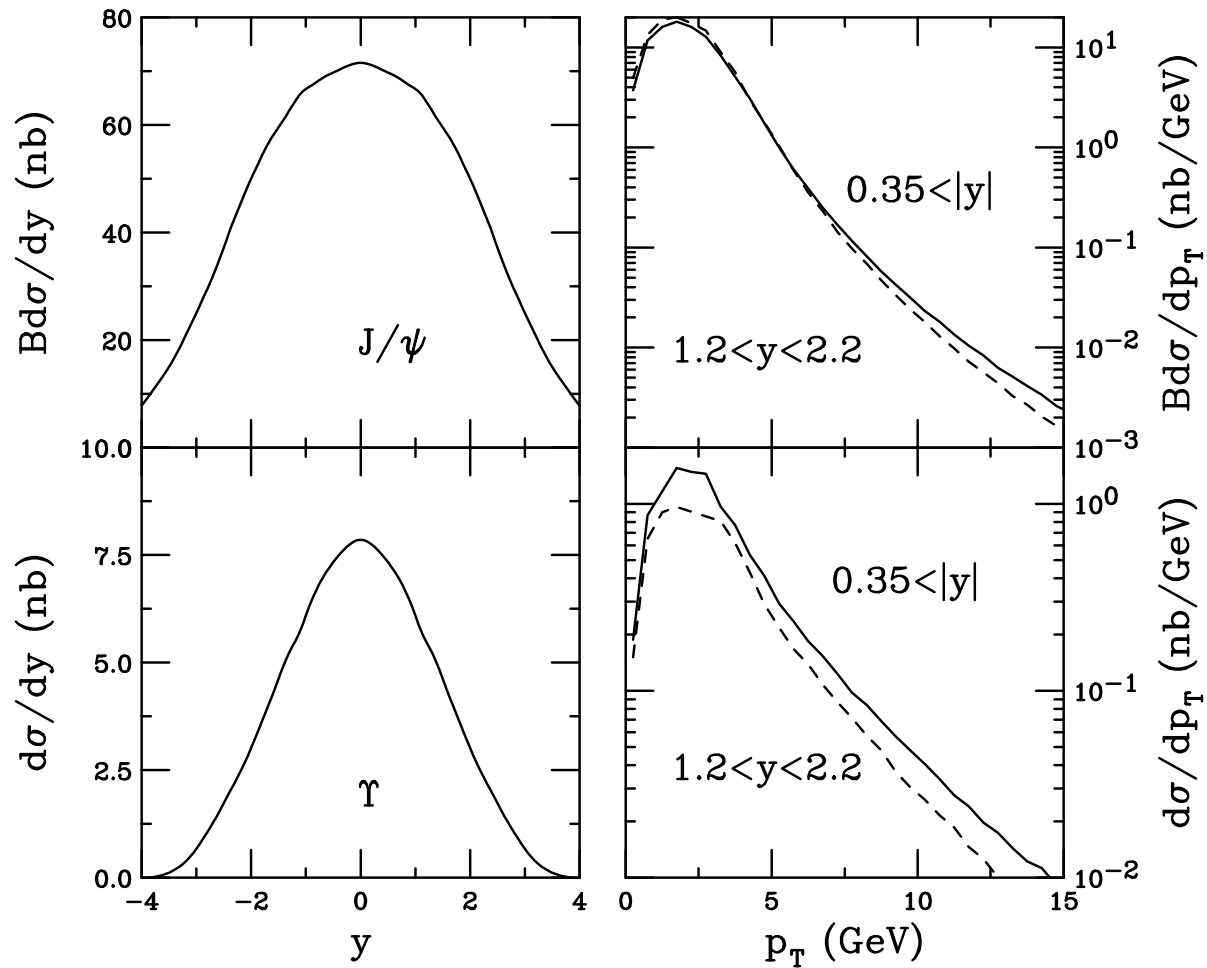


Figure 5: The inclusive  $J/\psi$  (top) and  $\Upsilon$  (bottom) rapidity (left) and  $p_T$  distributions (right) at  $\sqrt{s} = 500$  GeV. The  $p_T$  distributions at mid- and forward rapidity are shown.

# Polarization Crucial Test of Production Models

At large  $p_T$ , NRQCD quarkonium production dominated by gluon fragmentation into a color octet  $Q\bar{Q}$  ( $c\bar{c}[^3S_1^{(8)}]$ )

Fragmenting gluon is nearly on mass shell, thus transversely polarized; gluon polarization retained during hadronization but diluted by radiative corrections, color singlet production and feed down

Agreement not improved by newer, higher  $p_T$  Tevatron Run II data

CEM cannot predict quarkonium polarization without having an exclusive polarized  $Q\bar{Q}$  calculation to start with

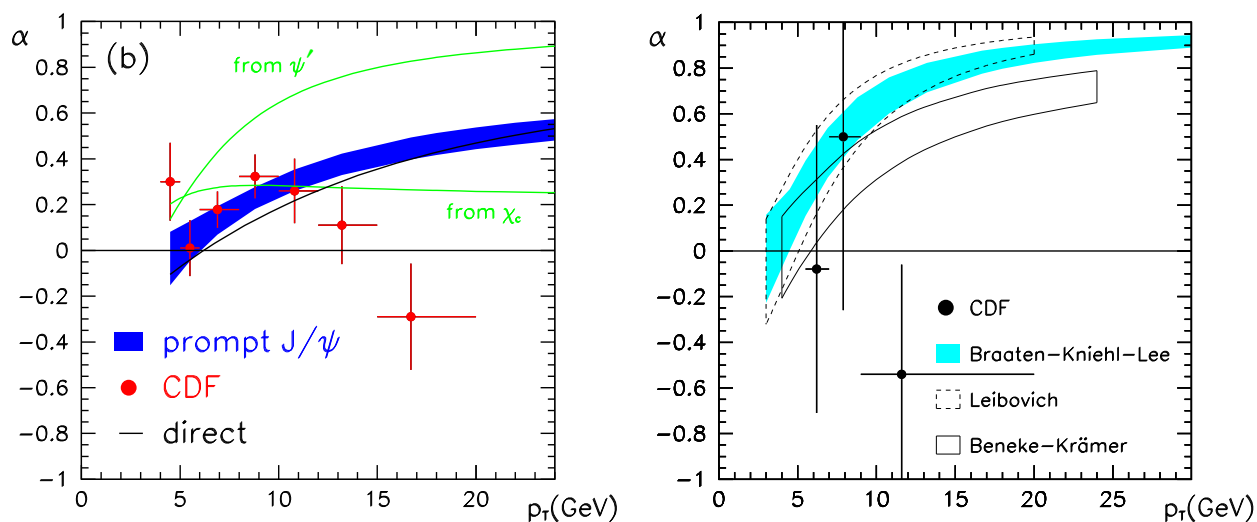


Figure 6: Left-hand side:  $J/\psi$  polarization at the Tevatron. The band is the total NRQCD-factorization prediction. The other curves give the contributions from feeddown from higher charmonium states. Right-hand side:  $\psi'$  polarization at the Tevatron. The bands give various NRQCD-factorization predictions. The data points are from the CDF measurement [Phys. Rev. Lett. **85** (2000) 2886]. From Braaten *et al.*, Phys. Rev. D **62** (2000) 094005.

# New Contributions to CSM: $s$ -cut Diagrams

Other box diagram contributions to CSM not previously considered, cut at  $\hat{s} = (k_1 + k_2)^2 \geq 4m_Q^2$ , uses  $m_Q > m_c/2$  to simplify calculation (CSM assumes  $m_c \geq 2m_Q$ )

Additional 4-point vertex (with fitted parameters) needed for gauge invariance while conserving current and not introducing additional singularities so the  $Q\bar{Q}$  pair forming quarkonium state  $\mathcal{C}$  is in a color octet state – only contributes to  $S$  state production, says nothing new about  $\chi_c$  states

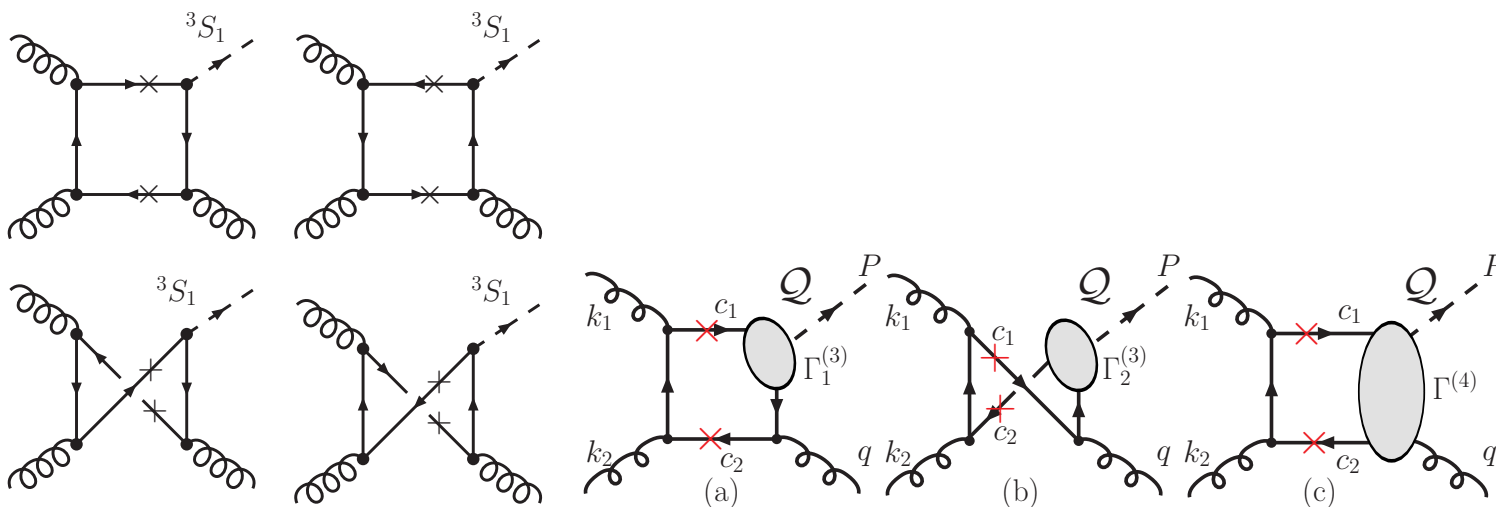


Figure 7: Left: Four diagrams representing the  $s$ -cut contribution to quarkonium production in the CSM. Right: (a,b) Leading-order (LO)  $s$ -channel cut diagrams contributing to  $gg \rightarrow Qq$  with direct and crossed box diagrams employing the  $c\bar{c}J/\psi$  vertex. The crosses indicate that the quarks are on-shell. (c) Box diagram with  $c\bar{c}Qq$  contact term mandated by gauge invariance.

# Effects of $s$ -Cut Contributions

Largest contribution to total cross section is from longitudinally polarized part – different from primarily transverse polarization of NRQCD

Can describe the CDF polarization data if  $\chi_c$  is assumed to be transversely polarized; agrees with RHIC  $J/\psi$  polarization at midrapidity but overpredicts polarization at forward rapidity [PHENIX, Quark Matter 2009]

$s$ -channel cut contributions tuned to fit CDF  $p_T$  distributions, RHIC shape and magnitude comes from phase space and energy dependence

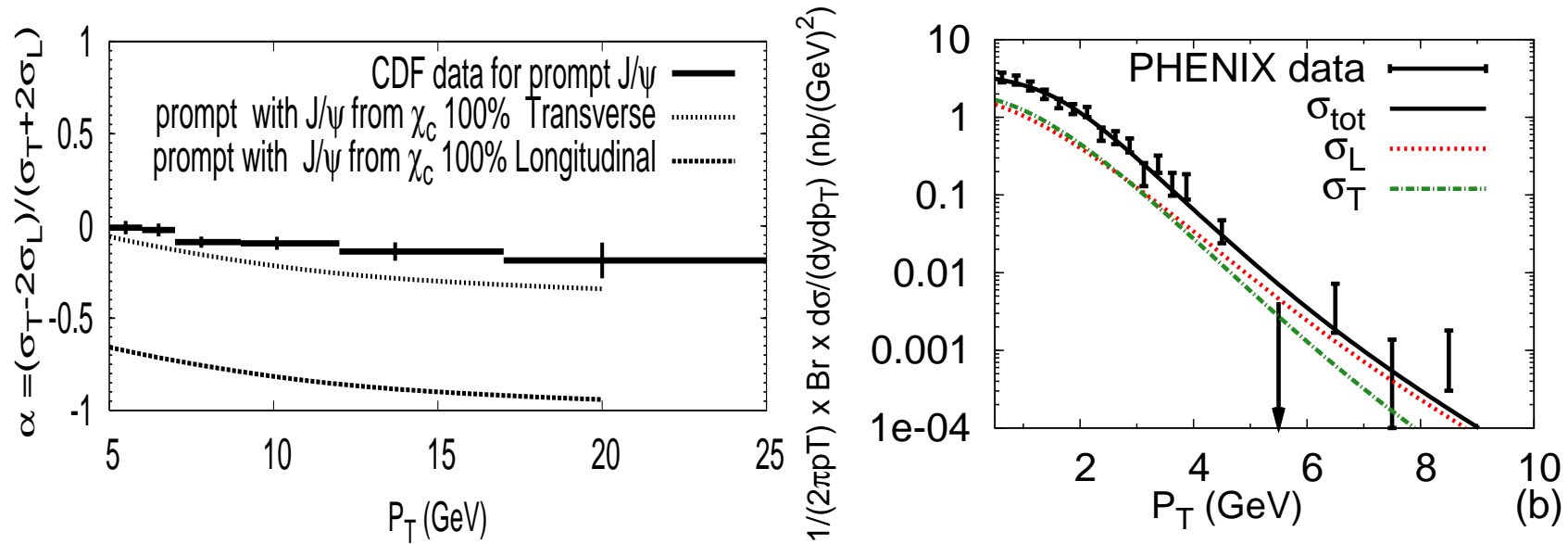


Figure 8: (Left) Comparison of  $\sigma_T$ ,  $\sigma_L$ ,  $\sigma_{\text{tot}}$  to PHENIX data [Phys. Rev. Lett. **98** (2007) 232002] ( $\sqrt{s} = 200$  GeV,  $|y| < 0.35$ ). (Right) Improved CSM calculation [Phys. Rev. Lett. **100** (2008) 032006] with two assumptions for two extremes of the polarization of prompt  $J/\psi$ 's from  $\chi_c$  decays: complete transverse (upper curve) and completely longitudinal (lower curve). The calculations are compared to the most recent CDF data [Phys. Rev. Lett. **99** (2007) 132001].

## *pA* and dA Production

# Medium Effects Important in $p(d)+A$ Interactions

Nuclear effects in fixed-target interactions

Parameterizing

$$\sigma_{pA} = \sigma_{pp} A^\alpha \quad \alpha(x_F, p_T)$$

For  $\sqrt{s_{NN}} \leq 40$  GeV and  $x_F > 0.25$ ,  $\alpha$  decreases strongly with  $x_F$  – only low  $x_F$  effects probed by SPS and RHIC rapidity coverage

Consider two low  $x_F$  cold matter effects at colliders:

- Nuclear Shadowing — initial-state effect on the parton distributions affecting total rate, important as a function of  $y/x_F$
- Absorption — final-state effect, after  $c\bar{c}$  that forms the  $J/\psi$  has been produced, pair breaks up in matter due to interactions with nucleons

At high  $x_F/y$ , other mechanisms (energy loss, intrinsic charm) may be important, to be discussed later

# Nuclear Modifications of the Parton Densities

# Nuclear Parton Distributions

Nuclear parton densities

$$\begin{aligned}F_i^A(x, Q^2, \vec{r}, z) &= \rho_A(s) S^i(A, x, Q^2, \vec{r}, z) f_i^N(x, Q^2) \\s &= \sqrt{r^2 + z^2} \\ \rho_A(s) &= \rho_0 \frac{1 + \omega(s/R_A)^2}{1 + \exp[(s - R_A)/d]}\end{aligned}$$

With no nuclear modifications,  $S^i(A, x, Q^2, \vec{r}, z) \equiv 1$

Assume spatial dependence proportional to nuclear path length:

$$S_\rho^i(A, x, Q^2, \vec{r}, z) = 1 + N_\rho(S^i(A, x, Q^2) - 1) \frac{\int dz \rho_A(\vec{r}, z)}{\int dz \rho_A(0, z)}$$

**Normalization:**  $(1/A) \int d^2r dz \rho_A(s) S_\rho^i \equiv S^i$ . Larger than average modifications for  $s = 0$ . Nucleons like free protons when  $s \gg R_A$ .

# Shadowing Parameterizations On The Market

- EKS98: K. J. Eskola, V. J. Kolhinen and P. V. Ruuskanen, Nucl. Phys. B 535 (1998) 351 [arXiv:hep-ph/9802350]; K. J. Eskola, V. J. Kolhinen and C. A. Salgado, Eur. Phys. J. C 9 (1999) 61 [arXiv:hep-ph/9807297].
- nDS: D. de Florian and R. Sassot, Phys. Rev. D 69, 074028 (2004) [arXiv:hep-ph/0311227].
- HKN: M. Hirai, S. Kumano and T. H. Nagai, Phys. Rev. C 70, 044905 (2004) [arXiv:hep-ph/0404093].
- FGS: L. Frankfurt, V. Guzey and M. Strikman, Phys. Rev. D 71 (2005) 054001 [arXiv:hep-ph/0303022].
- EPS08: K. J. Eskola, H. Paukkunen and C. A. Salgado, JHEP 0807, 102 (2008) [arXiv:0802.0139 [hep-ph]].
- EPS09: K. J. Eskola, H. Paukkunen and C. A. Salgado, JHEP 0904 (2009) 065 [arXiv:0902.4154 [hep-ph]].

## Differences Between Eskola *et al* Sets

**EKS98** Simple parameterization for all  $A$ ; leading order analysis only; GRV LO set used for proton PDFs; single set; **no  $\chi^2$  analysis performed**;  $2.25 \leq Q^2 \leq 10^4 \text{ GeV}^2$ ;  $10^{-6} < x < 1$

**EPS08** Simple parameterization for all  $A$ ; leading order analysis only; CTEQ61L set used for proton PDFs; single set;  **$\chi^2$  analysis uses forward BRAHMS data from RHIC to maximize gluon shadowing**;  $1.69 \leq Q^2 \leq 10^6 \text{ GeV}^2$ ;  $10^{-6} < x < 1$

**EPS09** Available for select  $A$  values; LO and NLO sets available based on CTEQ61L and CTEQ6M respectively;  **$\chi^2$  analysis done at both LO and NLO**; calling routine similar to other sets but now there are 31, 15 above and 15 below the central set; **no longer use BRAHMS data**

If  $\chi^2$ -minimized set of parameters,  $\{a_0\}$ , gives best estimate of nPDFs, work in a basis  $\{z\}$  that diagonalizes covariance matrix, errors in nPDFs computed within 90% confidence criteria,  $\Delta\chi^2 = 50$

Upper and lower uncertainties in any observable  $X$  can be computed using the prescription

$$\begin{aligned}(\Delta X^+)^2 &\approx \sum_k [\max\{X(S_k^+) - X(S^0), X(S_k^-) - X(S^0), 0\}]^2 \\(\Delta X^-)^2 &\approx \sum_k [\max\{X(S^0) - X(S_k^+), X(S^0) - X(S_k^-), 0\}]^2\end{aligned}$$

In all cases, when  $A$ ,  $x$  or  $Q^2$  are outside the range of validity, the last value is returned, *e.g.* if  $x < 10^{-6}$  value at  $x = 10^{-6}$  is given

# $Q^2$ Dependence of EPS09 – Constrains Gluon

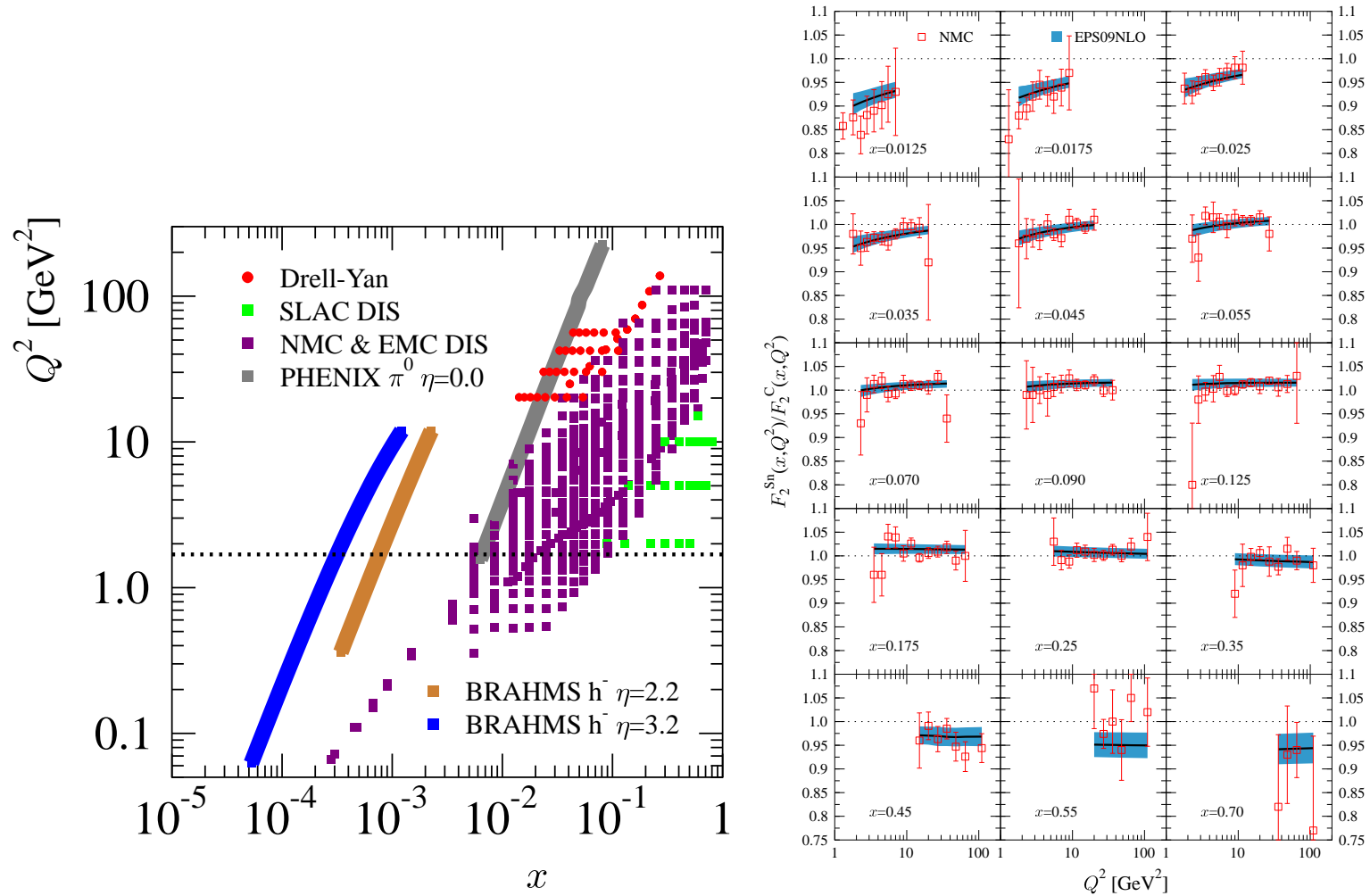


Figure 9: Left: initial gluon distributions at  $Q_0^2 = 1.4 \text{ GeV}^2$ . Right: evolution of gluon distributions for several fixed values of  $x$  shows that the effect of the nonlinear terms vanishes as  $Q^2$  increases.

## $x$ Dependence of EPS09

Note that the width of the uncertainty band can be bigger than any individual ratio since the errors added in quadrature

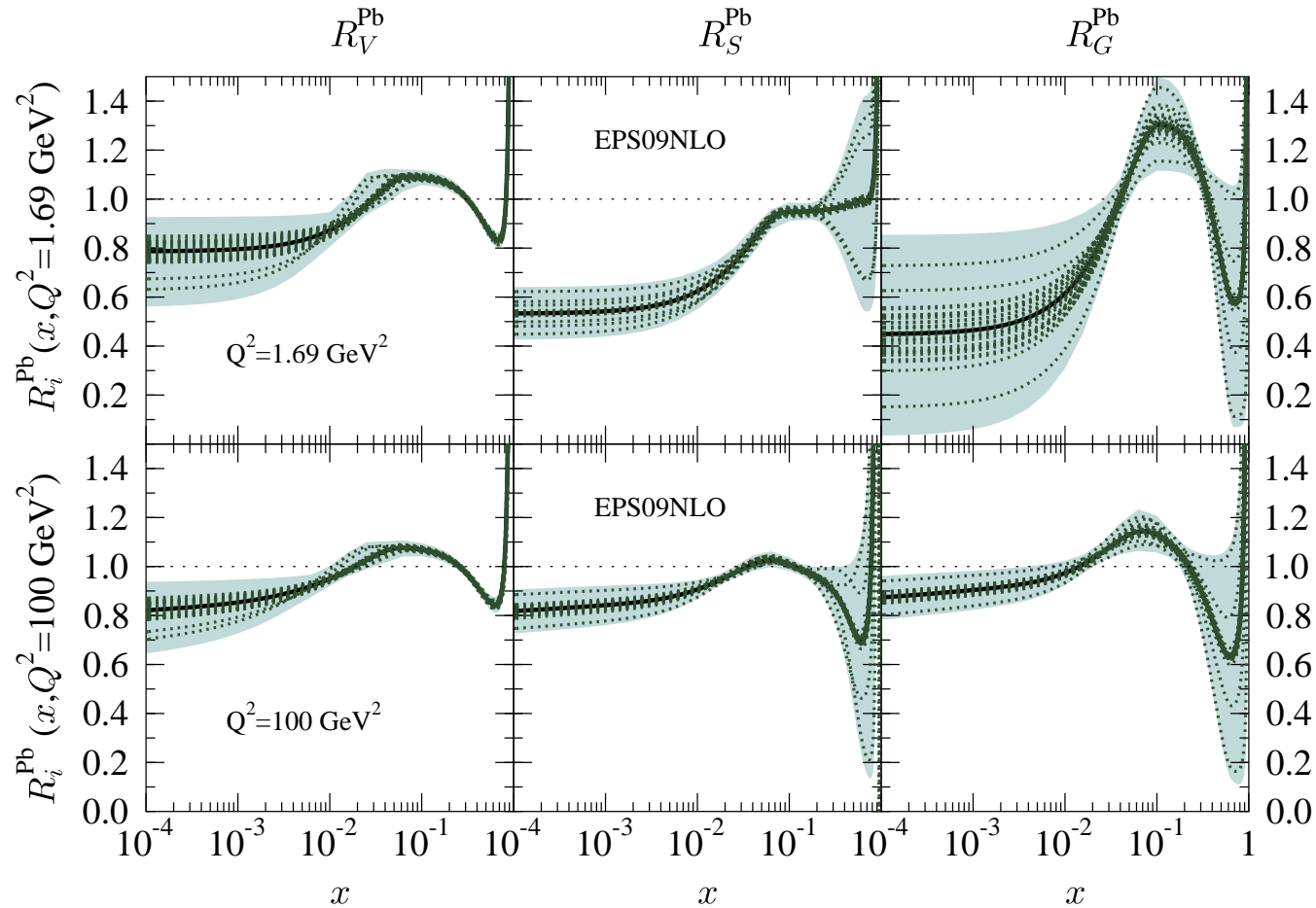


Figure 10: Left: initial gluon distributions at  $Q_0^2 = 1.4 \text{ GeV}^2$ . Right: evolution of gluon distributions for several fixed values of  $x$  shows that the effect of the nonlinear terms vanishes as  $Q^2$  increases.

# Comparison of LO and NLO nDS nPDFs

While the magnitude of the absolute cross sections may differ at LO and NLO, the effect of shadowing is, by design, the same at LO and NLO

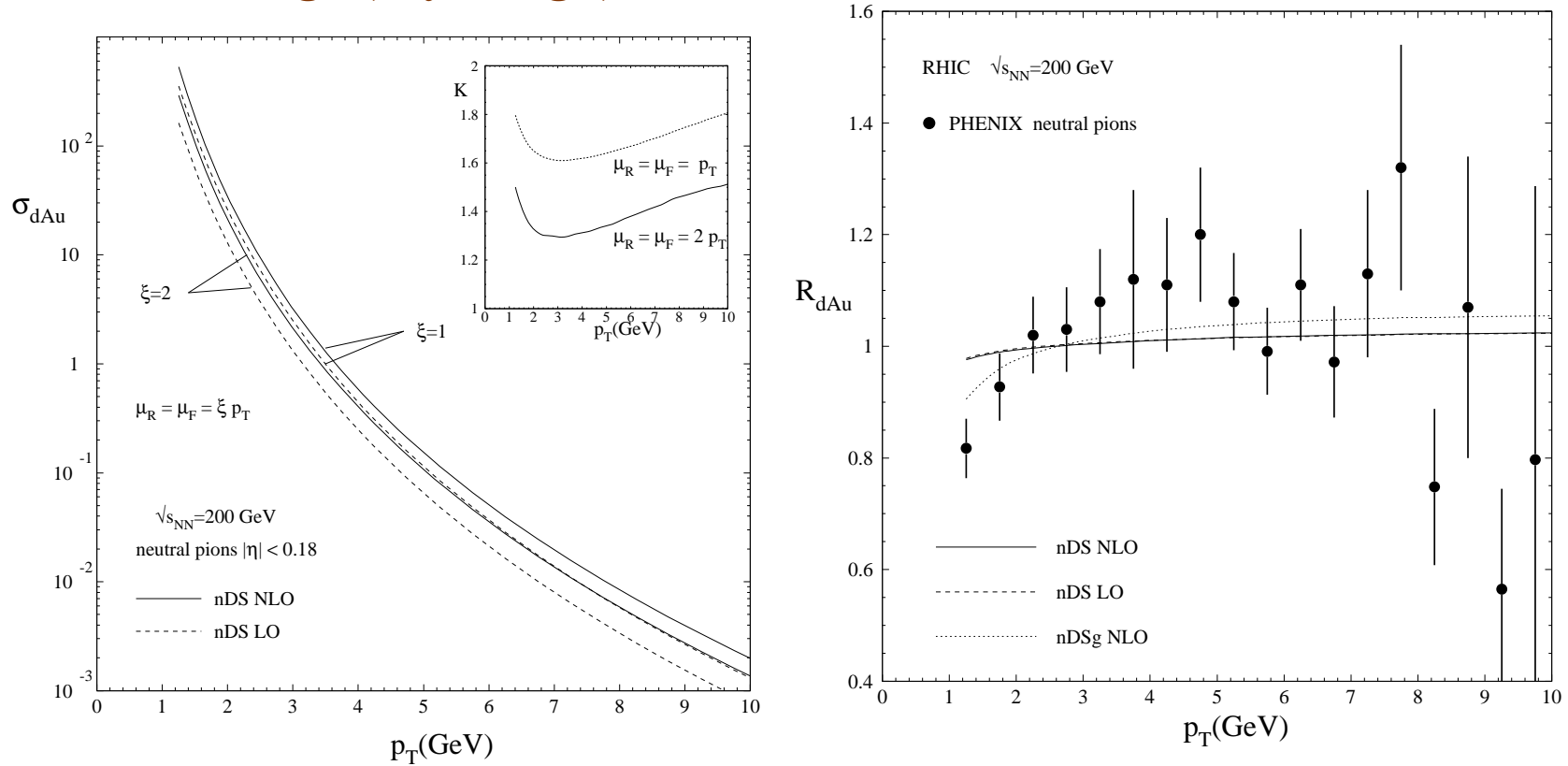


Figure 11: Left: The  $\pi^0$  cross section in d+Au collisions at  $\sqrt{s_{NN}} = 200$  GeV at LO and NLO. Right: The LO and NLO calculations of  $R_{dAu}$ .

# Comparing Shadowing Parameterizations: $x$ Dependence

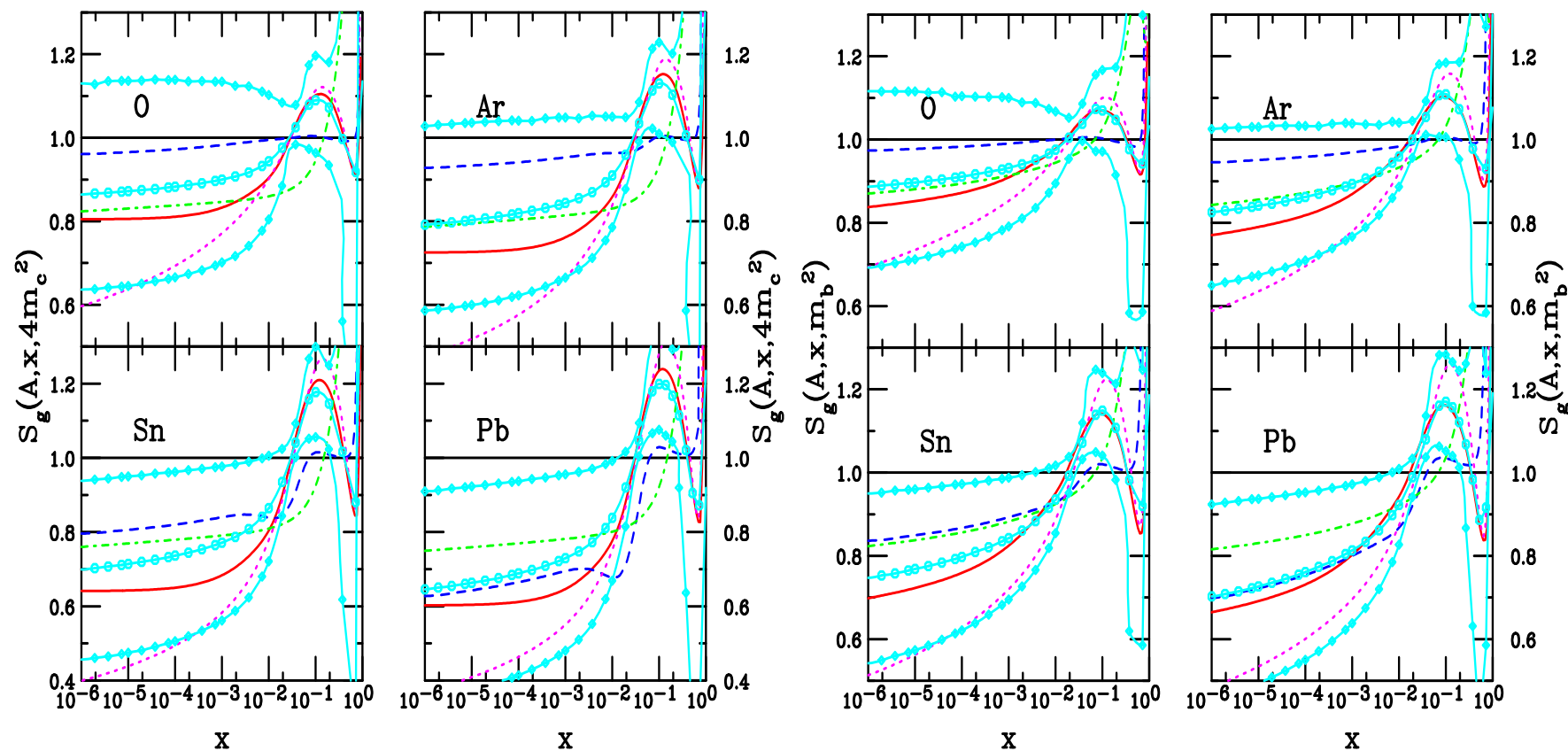


Figure 12: Comparison of EKS98 (red), nDSg (blue), HKN (green), EPS08 (magenta), and EPS09 (cyan, with symbols) gluon shadowing parameterizations for  $J/\psi$  (left) and  $\Upsilon$  (right) production scales with  $A=O, Ar, Sn$  and  $Pb$ .

# Predictions For $\Upsilon$ $R_{dAu}$ at RHIC

No absorption included

Larger  $x$  probed for  $\Upsilon$  production puts antishadowing peak near midrapidity, narrower  $y$  distributions than for  $J/\psi$  at same energy due to larger  $\Upsilon$  mass

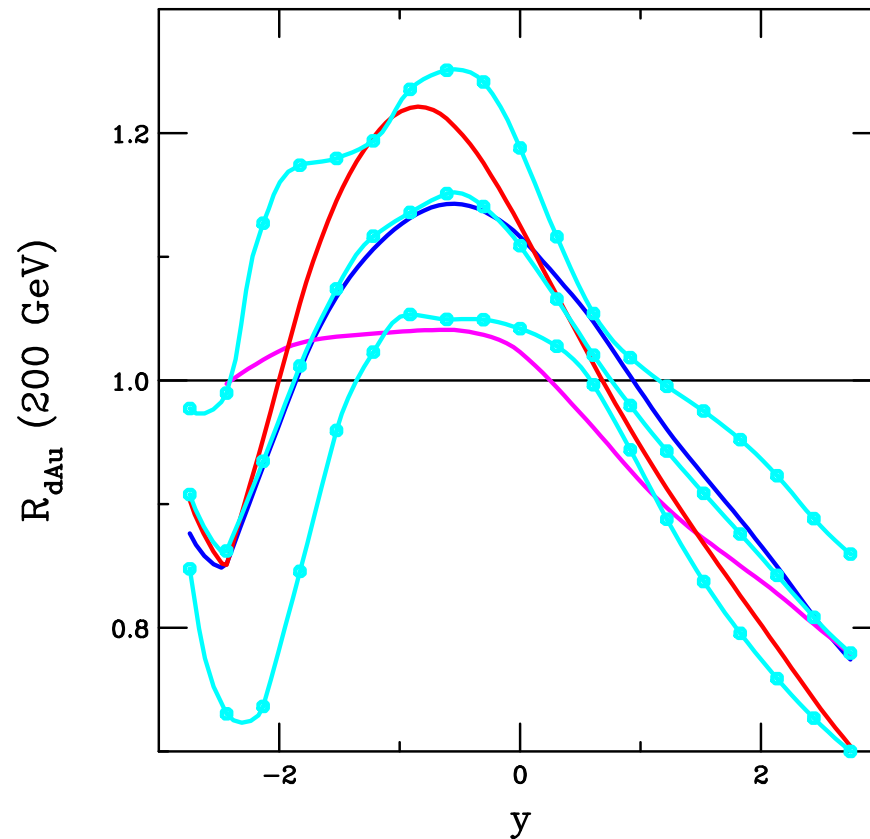


Figure 13: The d+Au/pp minimum bias ratios as a function of rapidity for the EKS98 (blue), nDSg (magenta), EPS08 (red) and EPS09 (cyan) parameterizations at 200 GeV.

# Kinematics of $J/\psi$ Production at Midrapidity

$pW/pp$  ratios of  $J/\psi$  production calculated with EKS98 and no final-state absorption

Left: Dependence on  $\sqrt{s_{NN}}$  at  $x_F = 0$ , energies of typical data indicated

Right: Dependence on  $x_F$  for three different energies; antishadowing peak narrows closer to  $x_F \sim 0$ ; shadowing stronger at forward  $x_F$

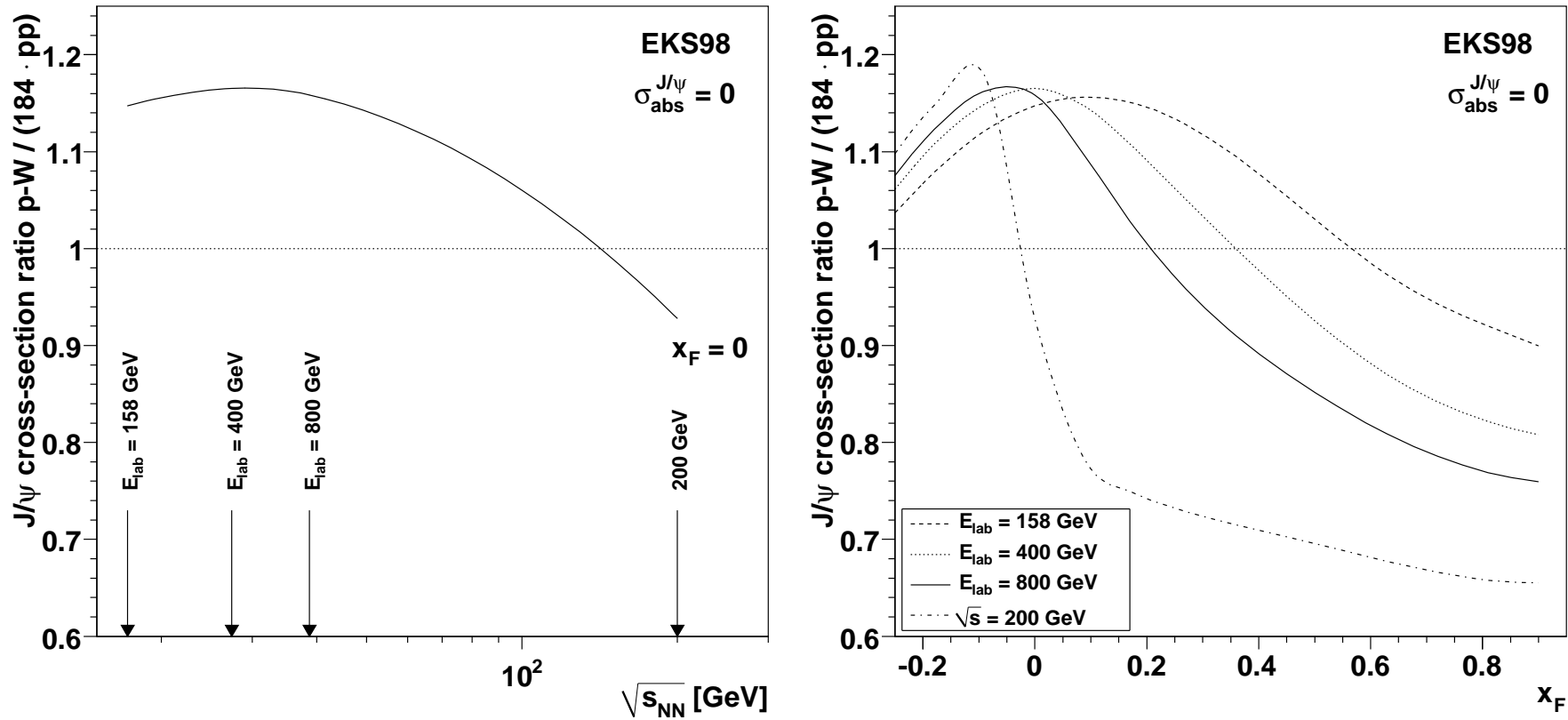


Figure 14: Changes induced by the nuclear modifications of the PDFs on the  $J/\psi$  production cross section per nucleon, in  $pW$  collisions, with EKS98, as a function of collision energy at  $x_F = 0$  (left) and as a function of  $x_F$  at three proton beam energies (right). [Lourenço, RV, Wöhri]

# Final-State Absorption

# Quarkonium Absorption by Nucleons

Woods-Saxon nuclear density profiles typically used

$$\begin{aligned}\sigma_{pA} &= \sigma_{pN} \int d^2b \int_{-\infty}^{\infty} dz \rho_A(b, z) S_A^{\text{abs}}(b) \\ &= \sigma_{pN} \int d^2b \int_{-\infty}^{\infty} dz \rho_A(b, z) \exp \left\{ - \int_z^{\infty} dz' \rho_A(b, z') \sigma_{\text{abs}}(z' - z) \right\}\end{aligned}$$

Note that if  $\rho_A = \rho_0$ ,  $\alpha = 1 - 9\sigma_{\text{abs}}/(16\pi r_0^2)$

The value of  $\sigma_{\text{abs}}$  depends on the parameterization of  $\sigma_{pA}$  – Glauber, hard sphere,  $A^\alpha$  etc. (shown by NA50)

Initial-state shadowing only recently taken into account at SPS energies,

Feed down to  $J/\psi$  from  $\chi_c$  and  $\psi'$  decays not always included, should dictate that

$$\sigma_{pA} = \sigma_{pN} \int d^2b [0.6S_{\psi, \text{dir}}(b) + 0.3S_{\chi_c J}(b) + 0.1S_{\psi'}(b)]$$

Assume that each charmonium state interacts with a different constant asymptotic absorption cross section

The  $\chi_c$   $A$  dependence remains unknown

# A Dependence of $J/\psi$ and $\psi'$ Not Identical

Color octet mechanism suggested that  $J/\psi$  and  $\psi'$   $A$  dependence should be identical — Supported by large uncertainties of early data

More extensive data sets (NA50 at SPS, E866 at FNAL) show clear difference at midrapidity [NA50  $\rho_L$  fit gives  $\Delta\sigma = \sigma_{\text{abs}}^{\psi'} - \sigma_{\text{abs}}^{J/\psi} = 4.2 \pm 1.0$  mb at 400 GeV,  $2.8 \pm 0.5$  mb at 450 GeV for absolute cross sections]

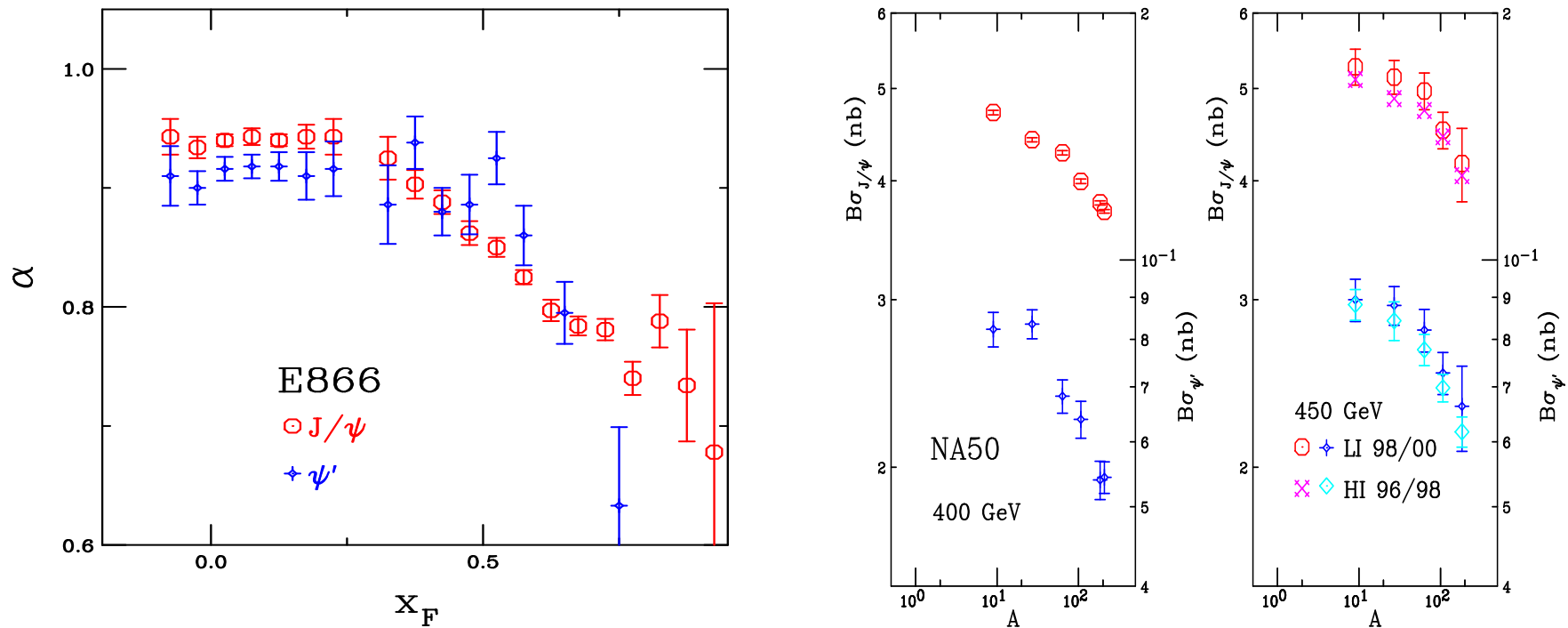


Figure 15: The  $J/\psi$   $A$  dependence (left) as a function of  $x_F$  at FNAL ( $\sqrt{s_{NN}} = 38.8$  GeV) and (right) and a function of  $A$  at the SPS (NA50 at  $p_{\text{lab}} = 400$  and 450 GeV) for  $J/\psi$  and  $\psi'$  production.

## Some Results and Some Speculations

# Interplay of Shadowing and Absorption

Depending on  $x$  values probed, shadowing can enhance or reduce absorption cross section needed to describe data

Absorption alone always gives less than linear  $A$  dependence ( $\alpha < 1$ )

For SPS energies,  $17.3 \leq \sqrt{s} \leq 29$  GeV, rapidity range covered is in EMC and antishadowing region,  $\alpha > 1$  with no absorption

Adding shadowing to SPS absorption calculations requires a larger absorption cross section to maintain agreement with data

For  $\sqrt{s} \geq 38$  GeV,  $x$  in shadowing regime, thus  $\alpha < 1$  with shadowing alone in forward region, reducing absorption cross section needed at midrapidity

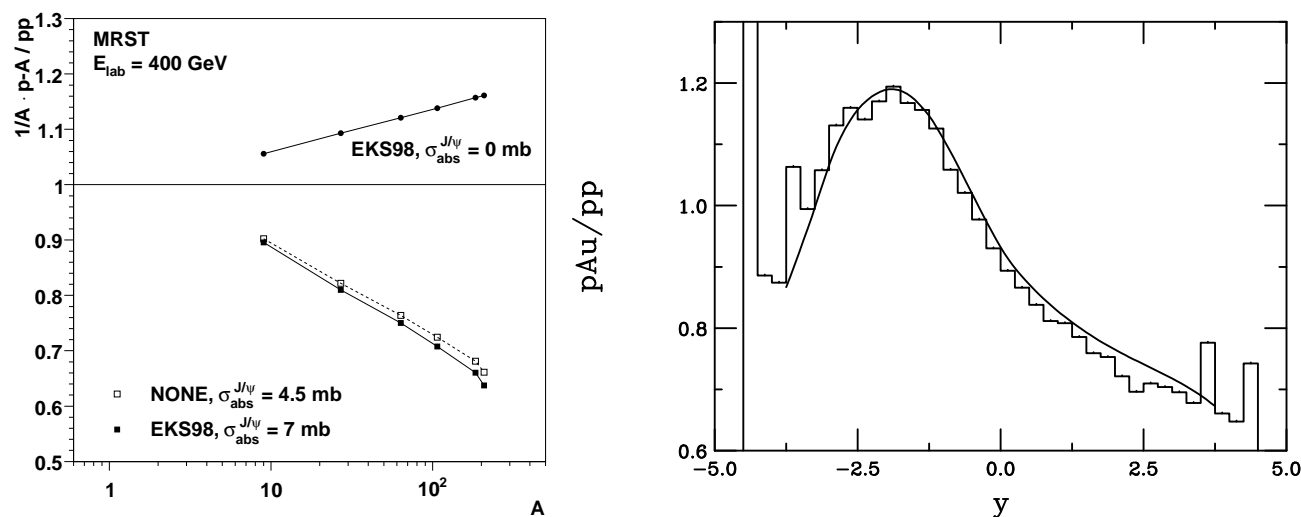


Figure 16: (Left) Illustration of the interplay between shadowing and absorption. [C. Lourenco, H. K. Woehri and RV, JHEP 0902 (2009) 014.] (Right) Comparison of LO and NLO shadowing ratios.

# Fit $\sigma_{\text{abs}}^{J/\psi}$ to Data and Extrapolate to Other Energies

Asymmetric Gaussians used to fit  $x_F < 0.25$  region of E866 and HERA-B data

Shapes at other energies determined by fits, magnitude adjusted to data:  $\sigma_{\text{abs}}^{J/\psi}$  seems to decrease with energy

Even with no shadowing effects included (left-hand side), there seems to be a systematic decrease of the absorption cross section with energy

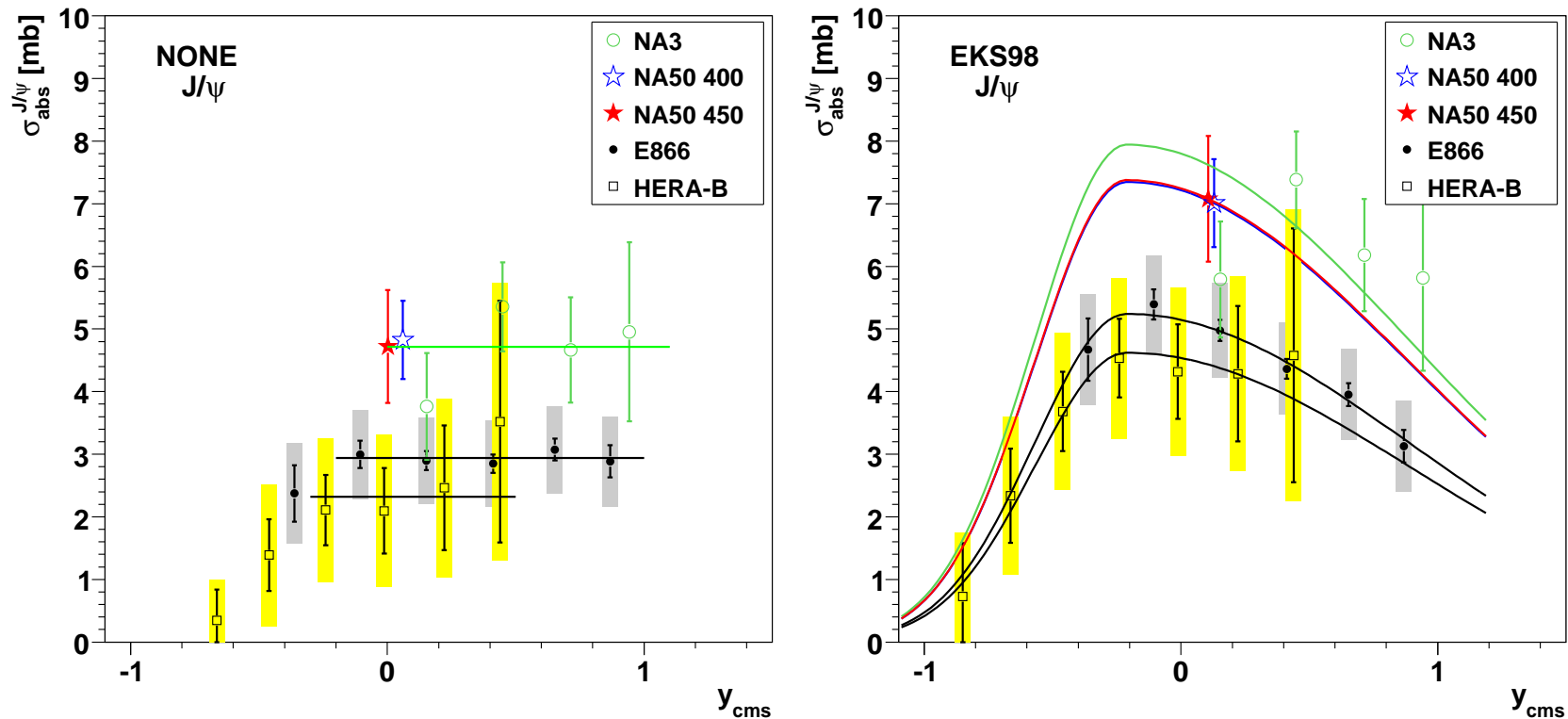


Figure 17: Dependence of  $\sigma_{\text{abs}}^{J/\psi}$  on  $y_{\text{cms}}$  for all available data sets. The shape of the curves is fixed by the E866 and HERA-B data. [Lourenço, RV, Wöhri] Left: Assuming no shadowing effects on the PDFs. Right: Including EPS98 shadowing.

# Quantifying Energy Dependence of $\sigma_{\text{abs}}^{J/\psi}$

$\sigma_{\text{abs}}^{J/\psi}(y_{\text{cms}} = 0)$  decreases with  $\sqrt{s_{NN}}$

$\sigma_{\text{abs}}^{J/\psi}(y_{\text{cms}} = 0)$  extrapolated to 158 GeV is significantly larger than measured at 450 GeV, underestimating “normal nuclear absorption” in SPS heavy-ion data

Calculations confirmed by NA60  $pA$  measurements at 158 GeV (QM09)

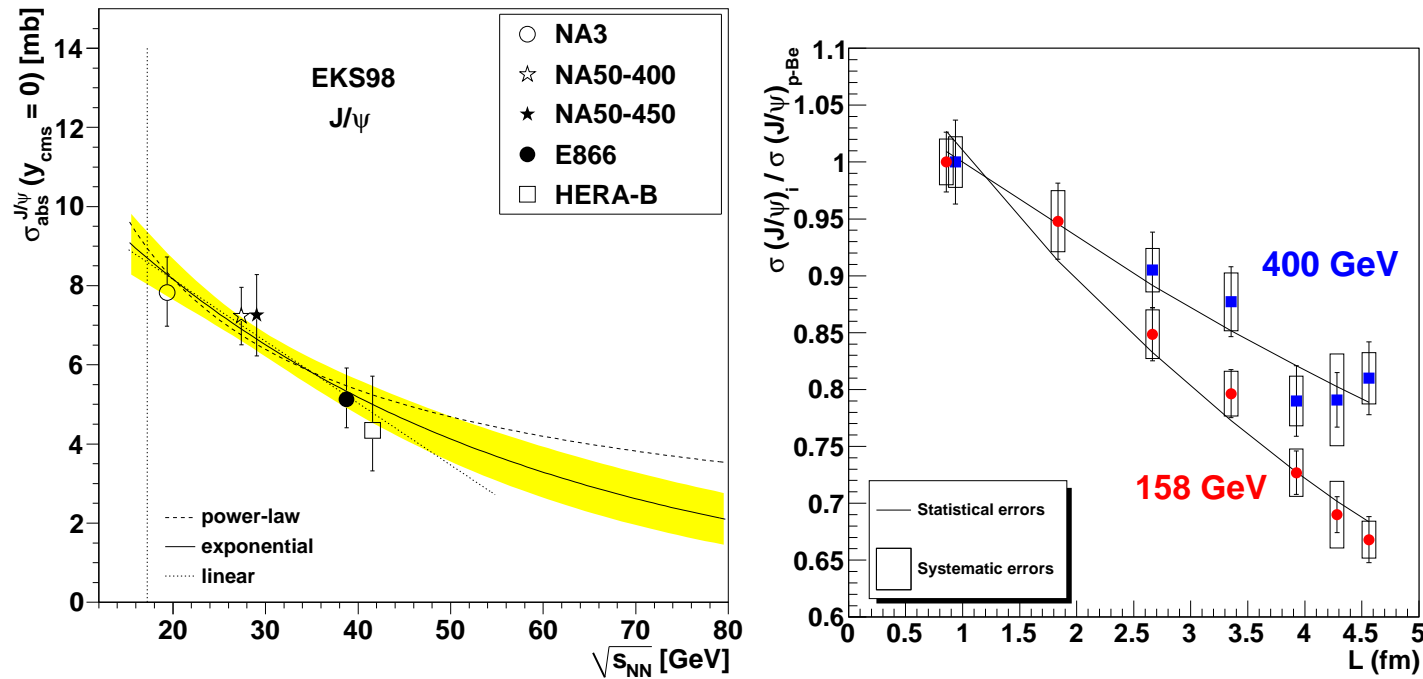


Figure 18: Left: The extracted energy dependence of  $\sigma_{\text{abs}}^{J/\psi}$  at midrapidity for power law (dashed), exponential (solid) and linear (dotted) approximations to  $\sigma_{\text{abs}}^{J/\psi}(y = 0, \sqrt{s_{NN}})$  using the EKS98 shadowing parameterization with the CTEQ61L parton densities. The band around the exponential curve indicates the uncertainty in the extracted cross sections at  $x_F \sim 0$  from NA3, NA50 at 400 and 450 GeV, E866 and HERA-B. The vertical dotted line indicates the energy of the Pb+Pb and In+In collisions at the CERN SPS. [Lourenço, RV, Wöhri] Right: The  $J/\psi$  cross section ratios for  $pA$  collisions at 158 GeV (circles) and 400 GeV (squares), as a function of  $L$ , the mean thickness of nuclear matter traversed by the  $J/\psi$ . [Arnaldi, Cortese, Scomparin]

# $x_F$ Dependence of $\sigma_{\text{abs}}^{J/\psi}$ Shows Holes in Our Understanding

Forward  $x_F$  ( $y_{\text{cms}}$ ) data more complex: strongly increased absorption in this region  
 NA60 data begin to rise at lower  $x_F$  than do higher energy results from E866 and PHENIX

Such strong effects can't come from any of the shadowing parameterizations shown before; we are investigating effects of energy loss but first need to set the possible quark energy loss level in NLO DY production, work in progress with C. Lorencio, H. Wöhri and P. Faccioli

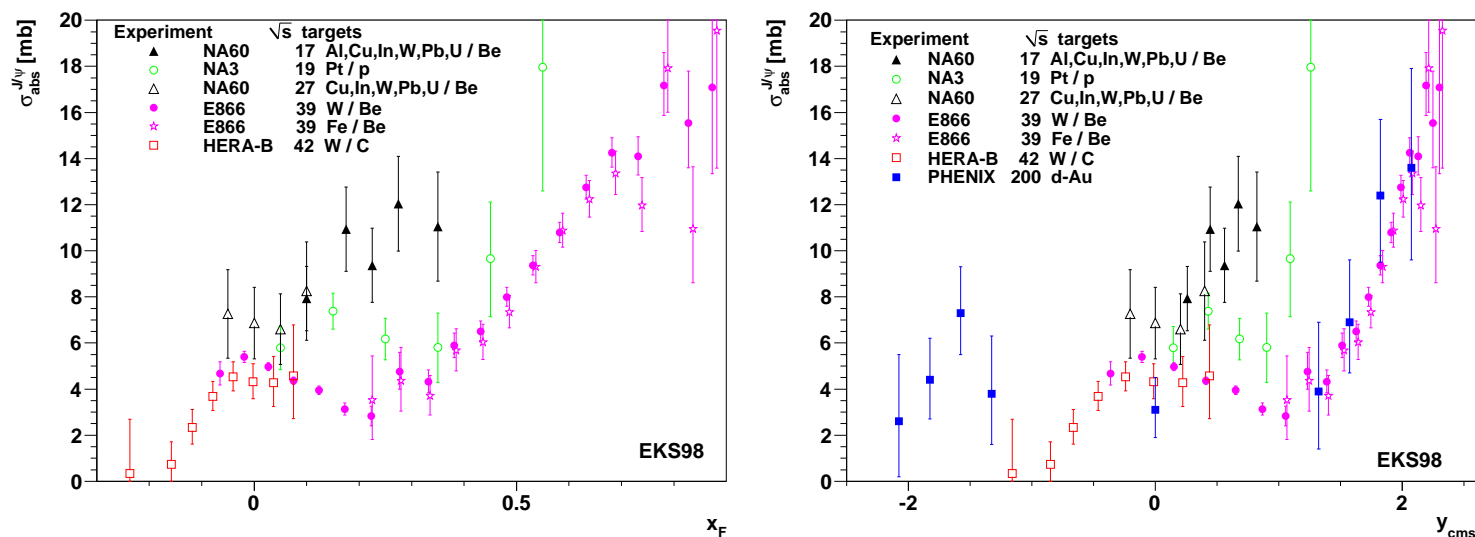


Figure 19: Left: The  $x_F$  dependence of  $\sigma_{\text{abs}}^{J/\psi}$  for incident fixed-target energies from 158, 200, 400, 450, 800 and 920 GeV obtained using the EKS98 shadowing parameterization. Right: The same results as above but as a function of center-of-mass rapidity  $y_{\text{CMS}}$ . The absorption cross sections extracted from the preliminary PHENIX results at  $|y_{\text{CMS}}| > 0$  and the central rapidity result are also included. [Plots made by Hermine Wöhri with PHENIX data from Tony Frawley.]

# Experimental Heavy/Light Ratios Confirm Effect

Rather wide range of EPS09 uncertainty reduced in ratios; clearly initial-state shadowing must be supplemented by other mechanisms

Away from midrapidity, the  $J/\psi$  and open charm measurements behave similarly, as might be expected from an initial-state effect

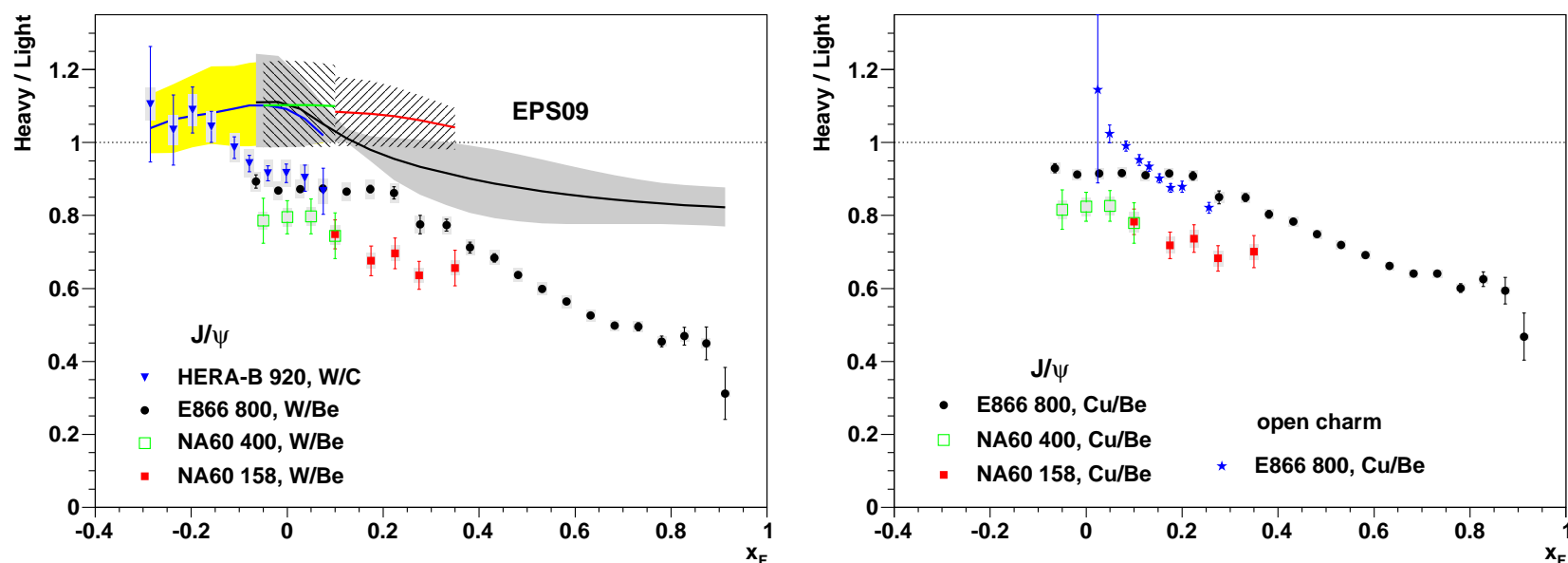


Figure 20: The heavy to light ratios for W/Be (left) as well as for Fe/Be and Cu/Be (right) in fixed target interactions. The right-hand figure also includes preliminary E866 open charm data.

# Including Initial-State Energy Loss

Combination of shadowing and energy loss with relatively  $x_F$ -independent absorption compares relatively well with the data for  $x_F > 0.2$

Stronger absorption closer to target? Formation time effects not yet considered

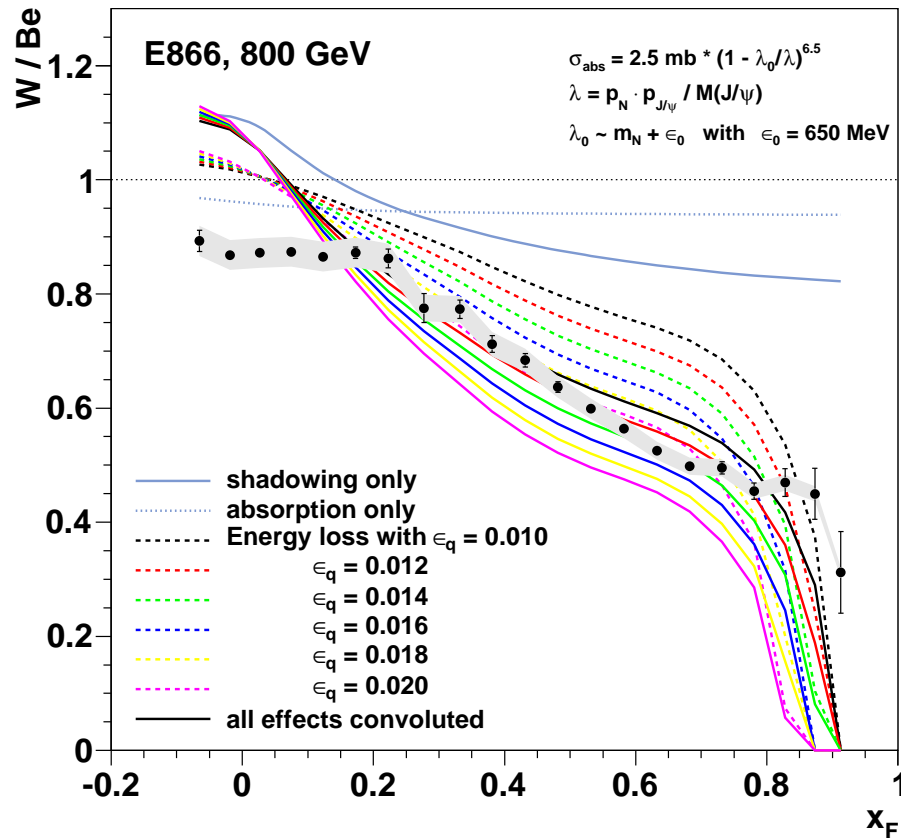


Figure 21: Convolution of shadowing, absorption and various strengths of initial-state energy loss by quarks compared to the E866 data.

## Summary .

- CEM agrees well with RHIC data; useful tool for studying cold nuclear matter effects .
- Data seem to suggest absorption cross section decreases with  $\sqrt{s_{NN}}$  and increases at forward  $x_F$ , work in progress, including formation time effects, initial-state energy loss, to understand why